Heterogeneous Catalysis

DOI: 10.1002/anie.201103798

Determining the Behavior of RuO_x Nanoparticles in Mixed-Metal Oxides: Structural and Catalytic Properties of $RuO_2/TiO_2(110)$ Surfaces**

*Fan Yang, Shankhamala Kundu, Alba B. Vidal, Jesús Graciani, Pedro J. Ramírez, Sanjaya D. Senanayake, Dario Stacchiola, Jaime Evans, Ping Liu, Javier Fdez Sanz, and José A. Rodriguez**

Dedicated to the Fritz Haber Institute, Berlin, on the occasion of its 100th anniversary

In recent years there has been a strong interest in obtaining a fundamental understanding of the chemical behavior of mixed-metal oxides at the nanometer range.[1–5] Studies involving the deposition of nanoparticles and clusters of VO_x, CeO_x, and WO_x on $TiO_2(110)$ and other well-defined oxide surfaces have shown novel structures that have special chemical properties.[1–3] Dimers of vanadia and ceria have been found on $TiO_2(110)$, monomers, trimers, and oligomers of vanadia on $CeO_2(111)$, and $(WO_3)_3$ clusters on TiO_2-(110).[1–3,6] In principle, the combination of two metals in an oxide matrix could produce materials with distinct catalytic activity or selectivity.[1,6–9] Herein, we use scanning tunneling microscopy (STM), X-ray photoelectron spectroscopy (XPS), and density functional (DF) calculations to study the interaction of RuO_2 nanostructures with $TiO_2(110)$. Our results show unique wire-like structures for RuO_2 that can be easily reduced and reoxidized. The special structural properties of $RuO_x/TiO_2(110)$ favor the dissociative adsorption of O_2 and the easy release of the adsorbed oxygen, making this mixed-metal oxide an excellent system for oxidation processes.

Figure 1a shows a STM image recorded after depositing $[Ru_3(CO)_{12}]$ on $TiO_2(110)$ at room temperature, with subsequent heating to 600 K to induce the cleavage of the Ru–CO bonds and evolution of CO into gas phase, and then exposure to O_2 at 550 K to form RuO_2 and remove any carbon that may have been deposited by the decomposition of CO. The complete transformation of $[Ru_3(CO)_{12}]$ into RuO_2 was verified in experiments of XPS (Supporting Information, Figure S1). Our results for the decomposition of the $[Ru_3(CO)_{12}]$ precursor are consistent with those reported in a previous study for the $[Ru_3(CO)_{12}]/TiO_2(110)$ system.[10] In Figure 1a, one-dimensional (1D) wire-like nanostructures can be seen elongated along the $<001>$ direction of the $TiO_2(110)$ substrate. These bright rows remained stable upon further annealing in 5×10^{-7} to 1×10^{-6} mbar O_2 at 600 K for 30 min. However, the 1D rows were not stable in ultrahigh vacuum (UHV). Upon further annealing above 650 K in UHV, we observed the appearance of bright clusters along these 1D rows. Further annealing at 750 K led to the disappearance of bright 1D rows and to the appearance of bright clusters (Supporting Information, Figure S2). At 850 K, most 1D rows disappeared from the surface except for those lying underneath the bright clusters. The Ru cluster size ranged from 2 to 5 nm. The cycle of oxidation–reduction shown in Figure 1 was repeated three times at temperatures between 550 K and 900 K. There was no detectable change in the density or height of surface Ru clusters, suggesting that diffusion of Ru into the bulk $TiO_2(110)$ was negligible.

The structure of the 1D RuO_2 rows was then considered (Figure 2). Since the oxidation of Ru cluster also exposes the TiO_2 substrate to O_2 at elevated temperatures, the reconstruction of $TiO_2(110)$ in O_2 should also be considered. It is known that interstitial Ti, which is mobile in the bulk, could diffuse to the surface of rutile TiO_2 at elevated temperatures and aggregate to form added rows of TiO_x.[11–14] Upon further oxidation, these rows arrange themselves into a cross-linked (1×2) structure.[11–14] The presence of RuO_2 inhibited the formation of the cross-linked (1×2) reconstruction, as shown in Figure 1b. Instead, we only observed wire-like rows extending along the $\langle 001\rangle$ direction of $TiO_2(110)$. The structure of the RuO_2 rows is illustrated in detail in Figure 2. Figure 2a shows that there are two types of strands on the $RuO_2/TiO_2(110)$ surface. Here, we term the two types of strands as bright strands (BS) and dark strands (DS), depending on their apparent height. The DS are rare on the surface and appear uniform in height, with an apparent height

[*] Dr. F. Yang, Dr. S. Kundu, Dr. A. B. Vidal, Dr. S. D. Senanayake, Dr. D. Stacchiola, Dr. P. Liu, Dr. J. A. Rodriguez
Chemistry Department, Brookhaven National Laboratory
Upton, NY 11973 (USA)
E-mail: rodrigez@bnl.gov
Prof. J. Graciani, Prof. J. F. Sanz
Departamento de Química Física, Universidad de Sevilla
41012 Seville (Spain)
P. J. Ramírez, Prof. J. Evans
Facultad de Ciencias, Universidad Central de Venezuela
Caracas 1020A (Venezuela)

[**] The work at BNL was financed by the US Department of Energy (DOE), Office of Basic Energy Science (DE-AC02-98CH10086). DFT calculations were performed using the computing facilities at the Center for Functional Nanomaterials, BNL. J.E. thanks INTEVEP and IDB for research grants that made possible part of this work at the Universidad Central de Venezuela. The work carried out at Seville was funded by MICINN and the Barcelona Supercomputing Center—Centro Nacional de Super-computacion (Spain). A.B.V. is on a leave of absence from the Venezuelan Institute of Scientific Investigations (IVIC).

Supporting information for this article is available on the WWW under http://dx.doi.org/10.1002/anie.201103798.

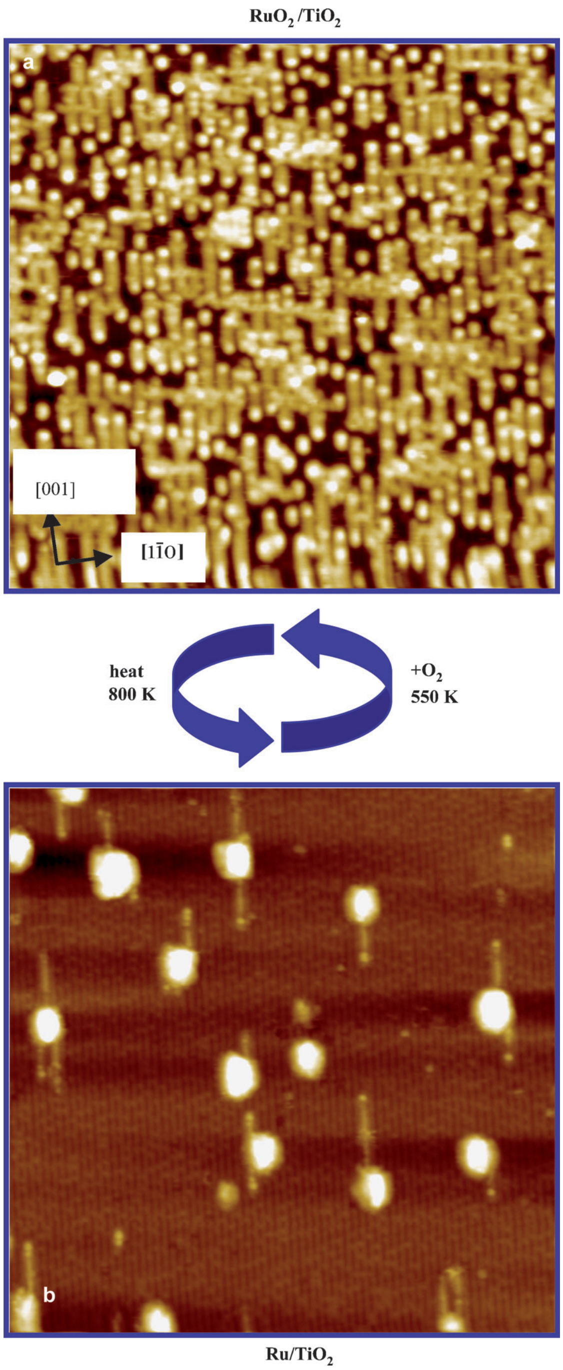

Figure 1. STM images of a) RuO$_2$/TiO$_2$ and b) Ru/TiO$_2$. The bright features in (b) correspond to 3D Ru nanoparticles. Reaction with O$_2$ at 550 K induces the formation of RuO$_2$, which transforms back into Ru upon heating above 800 K. Both images cover an area of 50 nm × 50 nm; $V_t = 2.1$ V, $I_t = 1.0$ nA.

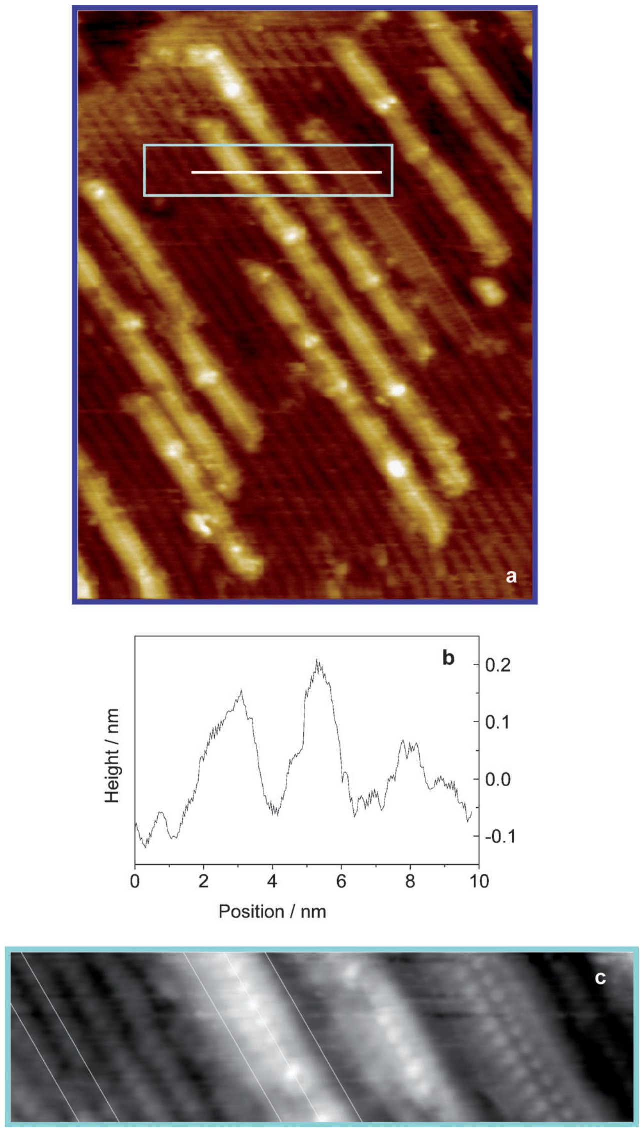

Figure 2. a) Wire-like structures for RuO$_2$ on TiO$_2$(110). Image size 30 nm × 20 nm. The inset compares in detail the structures found for 1D rows of RuO$_2$ and TiO$_x$. b) Height profile along the white line shown in (a). The two large peaks correspond to the bright rows, which contain RuO$_2$, whereas the small peak comes from a dark row of TiO$_x$. c) Close-up of the area inside of the white box in (a). To show the relative position of added rows with respect to the substrate, whites lines are imposed to mark the cus-Ti rows of TiO$_2$(110). The rows of RuO$_2$ and TiO$_x$ cover three regular rows of the TiO$_2$(110) substrate. $V_t = 1.5$ V, $I_t = 1.2$ nA.

of about 1.2 Å (Figure 2b). The BS, on the other hand, dominate the added rows on TiO$_2$(110) and appear inhomogeneous in height, with an apparent height of 2.2–3.0 Å (Figure 2b). Note that in previous studies on the (1 × 2) structure of TiO$_2$(110), two types of added TiO$_x$ rows were observed that differed depending on their height.[13–16] The higher strands have an apparent height 2.2–2.6 Å and the lower strands have an apparent height 1.2–1.5 Å. The STM image of the DS observed in our study exhibits three rows of bright dots running along the ⟨001⟩ direction. The structural features and the apparent height of the DS match exactly those of the added TiO$_x$ rows observed in the study by Iwasawa et al.[15] Thus,we assign the DS as added TiO$_x$ rows induced by the oxidation of TiO$_2$(110). On the other hand, the STM image of the BS cannot be matched with any STM image of the TiO$_x$ rows shown in previous studies. The higher strand of added TiO$_x$ rows typically displays two parallel rows of bright spots running along the ⟨001⟩ direction. In contrast, the BS observed in our study display a single row of bright spots centered in the strand (Figure 2c). Therefore, we propose that the BS seen here are formed by RuO_2 or a mixture of RuO_2 and TiO_x rows. Figure 2c also shows that the center of a bright strand is aligned with the cus-Ti rows of the TiO_2(110) substrate, and this strand has an apparent width of about 9 Å.

Using density-functional calculations, we investigated four possible structures for RuO_x on TiO_2(110), as shown in Figure 3. The RuO wire is similar to the TiO suboxide structure proposed by Park et al.[13] On the other hand, the Ru_3O_6-I wire is similar to the Ti_3O_6 unit proposed in previous studies[14,16,17] where the wire is composed of added RuO_2 strings with the troughs formed by RuO_2 vacancies. The Ru_3O_6-I and Ru_3O_6-II wires have the same number of Ru and O atoms bonded to different Ti and O sites of the titania substrate. The calculated order of stability follows the sequence: $RuO < Ru_2O_4 < Ru_3O_6\text{-II} \approx Ru_3O_6\text{-I}$, which is consistent with the fact that no wires with one or two rows of Ru (that is, the RuO and Ru_2O_4 models) were seen in our STM images. The calculated difference in the formation energies of Ru_3O_6-I and Ru_3O_6-II was small (ca. 0.2 eV), with Ru_3O_6-I being more stable. This type of structure is in excellent agreement with images found in STM, which show that each RuO_2 wire covers three rows of the TiO_2(110) substrate and exhibits bright protrusions at the wire center, probably as a consequence of a row of oxygen atoms located above Ru atoms.

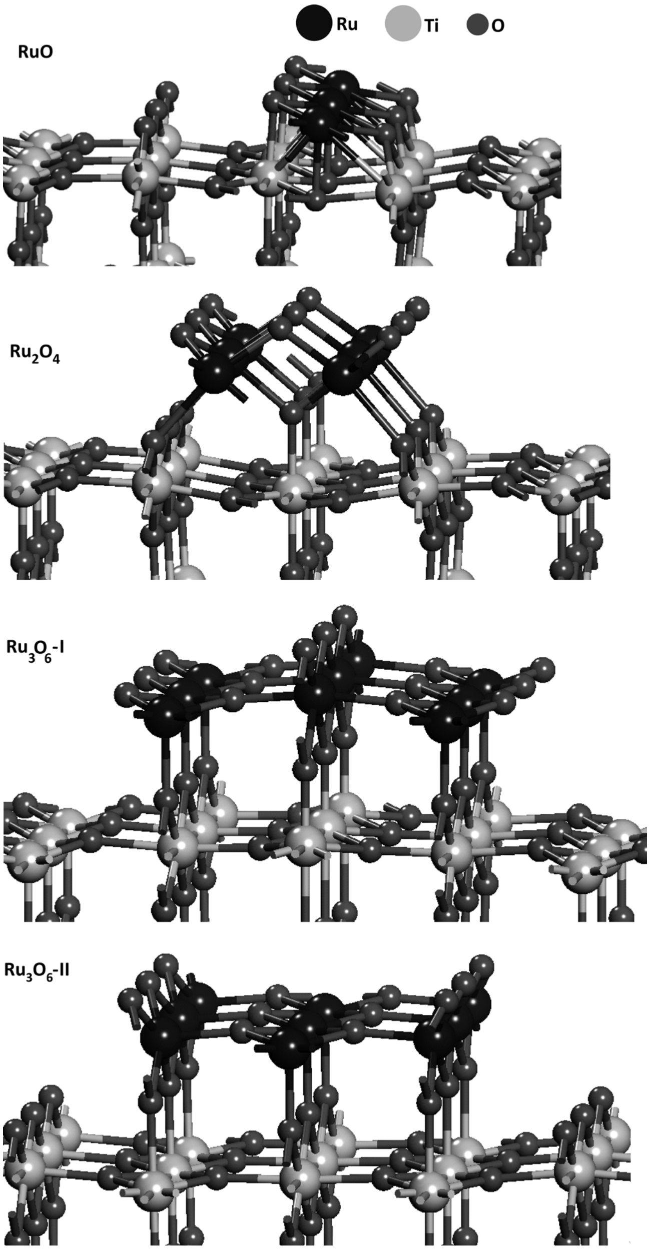

Figure 3. Models considered for the wire-like structures of RuO_x on TiO_2(110). The structures labeled RuO and Ru_3O_6-I are based on previous models proposed for the TiO_x/TiO_2(110) system.[13,14,16]

We used statistical thermodynamics[18,19] to take into account the effect of temperature, oxygen pressure, and ruthenium concentration on the stability of the ruthenium oxide wires on the TiO_2(110) surface. We calculated the change in the surface free energy $\Delta\gamma$ accompanying the Ru_xO_y formation:

$$x\,\text{Ru} + 0.5\,y\,\text{O}_2 + [\text{TiO}_2(110)] \leftrightarrow \text{Ru}_x\text{O}_y/[\text{TiO}_2(110)].$$

The calculated phase diagram in Figure 4 indicates that at 300 K and between UHV and atmospheric pressure, the

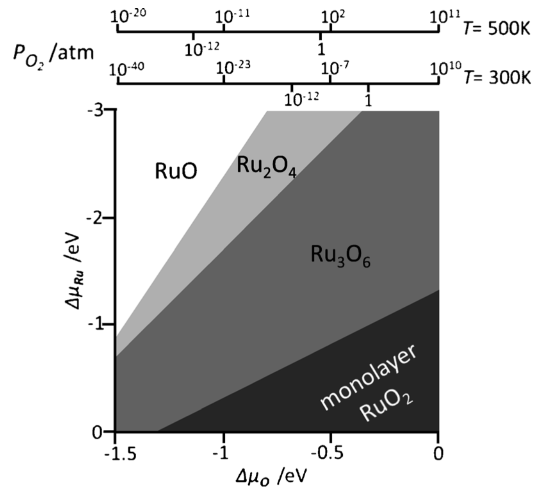

Figure 4. Calculated relative stability of the RuO/TiO_2(110), Ru_2O_4/TiO_2(110), and $Ru_3O_6\text{-I}/TiO_2$(110) phases as a function of the chemical potentials of Ru and O, the pressure of O_2, and the temperature of the system.

Ru_3O_6-I wire is the most stable for a wide range of Ru coverages. For very high Ru concentrations and high oxidizing conditions, a monolayer of bulklike RuO_2 is stable on top of TiO_2(110). Our calculations suggest that as the temperature increases under UHV pressure, Ru_3O_6 becomes unstable and starts to lose oxygen at temperatures above 500 K. This is in agreement with results of XPS and STM (Figure 1), which show the disappearance of the RuO_x wires at elevated temperatures and the formation of Ru nanoparticles.

Temperature and oxygen pressure had a dramatic effect on the elemental composition and morphology of the RuO_x/TiO_2(110) systems. Interestingly, the RuO_x nanostructures in contact with titania lose oxygen at much lower temperatures (700–850 K) than bulk RuO_2 (> 1000 K).[20] This property must be taken into consideration when preparing RuO_x/TiO_2 catalysts, as it can lead to large changes in catalytic activity or selectivity. In fact, this characteristic of RuO_x/TiO_2 may be the cause for the controversy that exists in the literature about the intrinsic activity of this material in photocatalytic processes.[8,9]

The $RuO_2/TiO_2(110)$ surfaces were more reactive towards CO than pure $TiO_2(110)$[21] or $RuO_2(110)$.[22] Figure 5 shows Ru 3d XPS spectra collected after dosing 300 L of CO to a

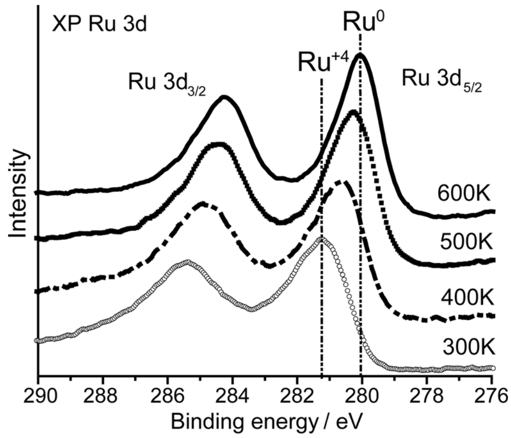

Figure 5. Ru 3d XPS spectra acquired after doses of 300 L of CO to a $RuO_2/TiO_2(110)$ surface at the indicated temperatures.

$RuO_2/TiO_2(110)$ surface at 300, 400, 500, and 600 K. Initially, the Ru 3d features exhibit the peak positions expected for RuO_2.[23] Upon exposure to CO at 400 K, there is a significant reduction of the RuO_2, and by 600 K only metallic Ru is present on the titania surface. The CO exposures used in these experiments would not reduce $TiO_2(110)$[21] or $RuO_2(110)$ significantly.[22]

The substantial reactivity of $RuO_x/TiO_2(110)$ towards CO and O_2 makes this system an excellent catalyst for the oxidation of CO. Figure 6 compares the CO oxidation activity of $TiO_2(110)$, $RuO_2/TiO_2(110)$, and $Au/TiO_2(110)$ surfaces at 350 K. Under these reaction conditions, namely a relatively low temperature and a stoichiometric ratio of CO and O_2, neither $TiO_2(110)$ nor $RuO_2(110)$ are active catalysts.[24,25] In contrast, titania surfaces with a 15–25 % coverage of RuO_2 exhibit activities comparable to the maximum activity of $Au/TiO_2(110)$, which is an excellent catalysts for CO oxidation.[25,26] This result is remarkable, as ruthenium is much less expensive than gold. Table 1 shows calculated (DF-GGA) reaction energy changes (ΔE) for the CO oxidation on $TiO_2(110)$ and on a model Ru_3O_6-I/$TiO_2(110)$ surface. On $TiO_2(110)$, we found a CO adsorption energy of only −0.19 eV, and the reaction energy for the formation of CO_2 was endothermic by 1 eV. In contrast, on the Ru_3O_6-I/$TiO_2(110)$ surface, the adorption energy of CO on a five-coordinate Ru site was −1.1 eV and the reaction energy for the formation of CO_2 was exothermic by 0.8 eV. From the experimental data (Figure 1 and Figure 5), low activation

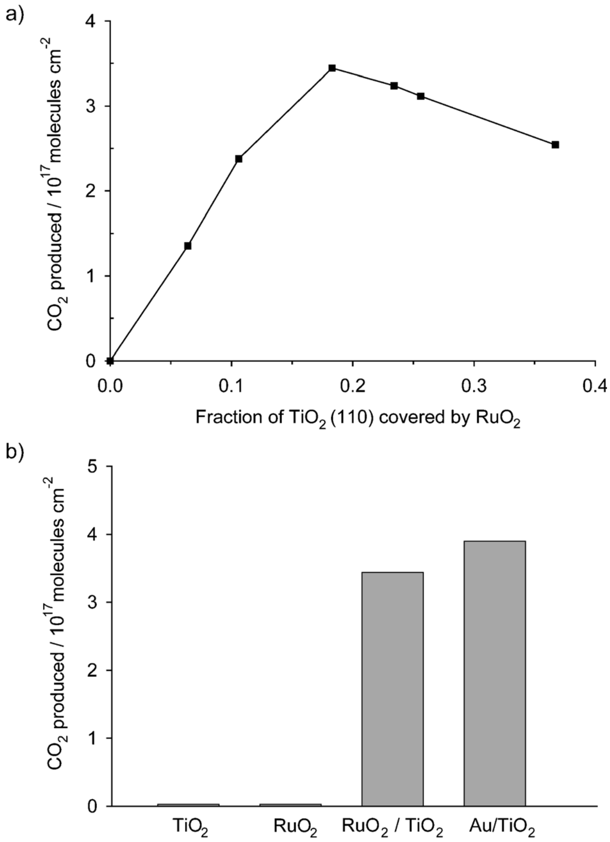

Figure 6. a) CO oxidation activity of $RuO_2/TiO_2(110)$ as a function of RuO_2 coverage. The area of the titania substrate covered by RuO_2 was measured by ion scattering spectroscopy before carrying out the oxidation of CO. The reported values for the production of CO_2 were obtained after exposing the catalysts to 4 Torr of CO and 2 Torr of O_2 at 350 K for 5 min. The number of CO_2 molecules produced is normalized by the sample surface area. b) Comparison of the activity for CO oxidation of clean $TiO_2(110)$, a $TiO_2(110)$ surface covered about 18 % by RuO_2, and a $TiO_2(110)$ surface with about 0.3 monolayers of Au. XPS showed only Ru^{4+} before and after CO oxidation.

Table 1: Energy changes calculated (DF-GGA) for the reaction $CO + 0.5\,O_2 \rightarrow CO_2$ on $TiO_2(110)$ and $Ru_3O_6/TiO_2(110)$ surfaces.

Reaction	ΔE [eV]
$TiO_2(110) + CO \rightarrow TiO_2(110)\text{-}O_{vac} + CO_2$	1.01
$TiO_2(110)\text{-}O_{vac} + 0.5\,O_2 \rightarrow TiO_2(110)$	−4.81
$Ru_3O_6/TiO_2(110) + CO \rightarrow Ru_3O_5/TiO_2(110) + CO_2$	−0.81
$Ru_3O_5/TiO_2(110) + 0.5\,O_2 \rightarrow Ru_3O_6/TiO_2(110)$	−2.99

barriers can be expected for these chemical processes. The special structural properties of $RuO_x/TiO_2(110)$ favor the dissociative adsorption of O_2 ($\Delta E = -2.99$ eV) and the easy release of oxygen present in the RuO_x lattice, making this surface an excellent catalyst for oxidation processes.

When compared to other systems that contain oxide nanoparticles dispersed on well-defined oxide substrates (VO_x on $TiO_2(110)$ or $CeO_2(111)$,[1,3,6] $(WO_3)_3$ on $TiO_2(110)$,[2] CeO_x on $TiO_2(110)$[26]), it is found that, despite the high stability of bulk RuO_2, $RuO_x/TiO_2(110)$ is the only mixed-metal oxide system in which the oxide overlayer is easily reduced to a metallic state. Thus, by taking advantage of the complex interactions that occur in a mixed-metal oxide at the nanometer level, materials can be engineered that have unique chemical properties.

Experimental Section

Microscopy studies were carried out in an Omicron variable temperature STM system.[26] Tungsten tips were used for imaging. Additional characterization studies were carried out at the photoemission endstations of beamlines U7A and U12 of the National Synchrotron Light Source (NSLS), and in a system which combines a batch reactor and a UHV chamber.[26] This UHV chamber (base pressure ca. 1×10^{-10} Torr) was equipped with instrumentation for X-ray photoelectron spectroscopy (XPS), low-energy electron diffraction, ion-scattering spectroscopy (ISS), and thermal-desorption mass spectrometry. For the photoemission experiments in U7A and U12, photon energies in the range of 400–650 eV were used. Clean TiO_2(110) surfaces were prepared by repeated cycles of argon-ion sputtering and annealing.[12,26] [$Ru_3(CO)_{12}$] vapor was introduced to the chamber by a doser, raising the chamber pressure to 1×10^{-8} Torr. While dosing, the TiO_2 crystal was at 300 K. The area of the titania surface covered by RuO_x was estimated using STM images or a combination of ISS and XPS. In the {UHV chamber + reactor} system, the RuO_x/TiO(110) sample could be transferred between the UHV chamber and reactor without exposure to air. Typically, it was transferred to the batch reactor at about 300 K, the reactant gases were introduced (4 Torr of CO and 2 Torr of O_2), and then the sample was rapidly heated to the reaction temperature of 350 K. The amount of molecules produced was normalized by the active area exposed by the sample. In our reactor, a steady-state regime for the production of CO_2 was reached after about 2 min of reaction time.

Periodic DFT calculations were performed with the VASP code[27] using a (1×2) six-layer thick supercell to model the TiO_2 (110) surface. In this model the two lowest layers were fixed at the optimized atomic bulk positions while atoms in the upper four layers were allowed to relax. We used the Perdew–Wang 91 GGA functional for exchange correlation, the projector-augmented wave approach, and plane waves with a cutoff energy set at 400 eV. We treated the Ti(3s,3p,3d,4), Ru(4d,5s), C(2s,2p), and O(2s,2p) electrons as valence states, while the remaining electrons were kept frozen as core states. Following the approach originally developed by Reuter and Scheffler,[19] we used statistical thermodynamics to take into account the effect of temperature, oxygen pressure, and ruthenium concentration on the stability of different ruthenium oxide species on the TiO_2 (110) surface. Additional details of the experimental and theoretical methods are provided in Supporting Information.

Received: June 4, 2011
Revised: July 4, 2011
Published online: September 13, 2011

Keywords: CO oxidation · heterogeneous catalysis · nanocatalysts · ruthenium oxide · titania

[1] J. A. Rodriguez, D. Stacchiola, *Phys. Chem. Chem. Phys.* **2010**, *12*, 9557 – 9565.
[2] O. Bondarchuk, X. Huang, J. Kim, B. D. Kay, L.-S. Wang, J. M. White, Z. Dohnálek, *Angew. Chem.* **2006**, *118*, 4904 – 4907; *Angew. Chem. Int. Ed.* **2006**, *45*, 4786 – 4789.
[3] M. Baron, H. Abbot, O. Bondarchuk, D. Stacchiola, A. Uhl, S. Shaikhutdinov, H.-J. Freund, C. Popa, M. V. Ganduglia-Pirovano, J. Sauer, *Angew. Chem.* **2009**, *121*, 8150 – 8153; *Angew. Chem. Int. Ed.* **2009**, *48*, 8006 – 8009.
[4] I. Muylaert, P. Van Der Voort, *Phys. Chem. Chem. Phys.* **2009**, *11*, 2826 – 2832.
[5] G. Zhou, L. Barrio, S. Agnoli, S. D. Senanayake, J. Evans, A. Kubacka, M. Estrella, J. C. Hanson, A. Martínez-Arias, M. Fernández-García, J. A. Rodriguez, *Angew. Chem.* **2010**, *122*, 9874 – 9878; *Angew. Chem. Int. Ed.* **2010**, *49*, 9680 – 9684.
[6] M. V. Ganduglia-Pirovano, C. Popa, J. Sauer, H. Abbott, A. Uhl, M. Baron, D. Stacchiola, O. Bondarchuk, S. Shaikhutdinov, H. J. Freund, *J. Am. Chem. Soc.* **2010**, *132*, 2345 – 2349.
[7] a) N. M. Gupta, V. S. Kamble, R. M. Iyer, K. R. Thampi, M. Grätzel, *J. Catal.* **1992**, *137*, 473 – 486; b) V. S. Kamble, V. P. Londhe, N. M. Gupta, K. R. Thampi, M. Grätzel, *J. Catal.* **1996**, *158*, 427 – 438.
[8] S. Ogura, M. Kohno, K. Sato, Y. Inoue, *J. Mater. Chem.* **1998**, *8*, 2335 – 2337.
[9] a) B.-Y. Yao, L. M. Wang, C. Wang, Y.-X. Wnag, G.-Y. Zhao, *Chin. J. Chem. Phys.* **2007**, *20*, 789 – 795; b) K. Ikarashi, J. Sato, H. Kobayashi, N. Saito, H. Nishiyama, Y. Inoue, *J. Phys. Chem. B* **2002**, *106*, 9048 – 9053.
[10] D. C. Meier, G. A. Rizzi, G. Granozzi, X. Lai, D. W. Goodman, *Langmuir* **2002**, *18*, 698 – 705.
[11] C. Xu, X. Lai, G. W. Zajac, D. W. Goodman, *Phys. Rev. B* **1997**, *56*, 13464 – 13482.
[12] a) M. A. Henderson, *Surf. Sci.* **1999**, *419*, 174 – 187; b) U. Diebold, *Surf. Sci. Rep.* **2003**, *48*, 53 – 229.
[13] K. T. Park, M. Pan, V. Meunier, E. W. Plummer, *Phys. Rev. B* **2007**, *75*, 245415; K. T. Park, M. Pan, V. Meunier, E. W. Plummer, *Phys. Rev. Lett.* **2006**, *96*, 226105.
[14] M. Bowker, R. A. Bennett, *J. Phys. Condens. Matter* **2009**, *21*, 474224.
[15] a) S. Takakugasi, K. Fukui, F. Nariyuki, Y. Iwasawa, *Surf. Sci.* **2003**, *523*, L41 – L46; b) H. Onishi, Y. Iwasawa, *Phys. Rev. Lett.* **1996**, *76*, 791 – 794.
[16] R. A. Bennett, P. Stone, N. J. Price, M. Bowker, *Phys. Rev. Lett.* **1999**, *82*, 3831 – 3834.
[17] H. H. Pieper, K. Venkatarami, S. Torbrugge, S. Bahr, J. V. Lauritsen, F. Besenbacher, A. Kuhnle, M. Reichling, *Phys. Chem. Chem. Phys.* **2010**, *12*, 12436 – 12441.
[18] V. Brazdova, M. V. Ganduglia-Pirovano, J. Sauer, *J. Phys. Chem. C* **2010**, *114*, 4983 – 4994.
[19] K. Reuter, M. Scheffler, *Phys. Rev. B* **2001**, *65*, 035406.
[20] J. Assmann, V. Narkhede, N. A. Breuer, M. Muhler, A. P. Seitsonen, M. Knapp, D. Crihan, A. Farkas, G. Mellau, H. Over, *J. Phys. Condens. Matter* **2008**, *20*, 184017.
[21] A. Linsebigler, G. Lu, J. T. Yates, *J. Chem. Phys.* **1995**, *103*, 9438.
[22] S. H. Kim, U. A. Paulus, Y. Wang, J. Witterlin, K. Jacobi, G. Ertl, *J. Chem. Phys.* **2003**, *119*, 9729 – 9736.
[23] G. A. Rizzi, A. Magrin, G. Granozzi, *Phys. Chem. Chem. Phys.* **1999**, *1*, 709 – 711.
[24] F. Gao, Y. Wang, Y. Cai, D. W. Goodman, *Surf. Sci.* **2009**, *603*, 1126 – 1134.
[25] M. Valden, X. Lai, D. W. Goodman, *Science* **1998**, *281*, 1647 – 1650.
[26] J. B. Park, J. Graciani, J. Evans, D. Stacchiola, S. Ma, P. Liu, A. Nambu, J. F. Sanz, J. Hrbek and J. A. Rodriguez, *Proc. Natl. Acad. Sci. USA* **2009**, *106*, 4975 – 4980.
[27] G. Kresse, J. Furthmuller, *Comput. Mater. Sci.* **1996**, *6*, 15 – 50.

